



ELSEVIER

Available online at www.sciencedirect.com

SCIENCE @ DIRECT®

ISPRS Journal of Photogrammetry & Remote Sensing 58 (2004) 289–300

PHOTOGRAMMETRY
& REMOTE SENSING

www.elsevier.com/locate/isprsjprs

Extraction, modelling, and use of linear features for restitution of airborne hyperspectral imagery

Changno Lee^{a,*}, James S. Bethel^b

^a*Spacial Imagery Information Research Team, ETRI, 161 Gajeong-dong, Yuseong-gu, Daejeon, 305-350, South Korea*

^b*Geomatic Engineerings, 1284 Civil Engineering Building, Purdue University, West Lafayette, IN, USA*

Received 11 September 2000; accepted 9 October 2003

Available online 14 December 2003

Abstract

This paper presents an approach for the restitution of airborne hyperspectral imagery with linear features. The approach consisted of semi-automatic line extraction and mathematical modelling of the linear features. First, the line was approximately determined manually and refined using dynamic programming. The extracted lines could then be used as control data with the ground information of the lines, or as constraints with simple assumption for the ground information of the line. The experimental results are presented numerically in tables of RMS residuals of check points as well as visually in ortho-rectified images.

© 2003 Elsevier B.V. All rights reserved.

Keywords: HYDICE; hyperspectral; sensor modelling; platform modelling; linear features

1. Introduction

Although linear features are not widely used for sensor modelling of linear array scanner imagery, many experiments have proven the usefulness of linear features in sensor modelling of frame imagery (Mulawa, 1989; Sayed, 1990; Habib et al., 2000).

For conventional photogrammetry applications, linear features offer some advantages over control points in their use as control features. When used in overlapping imagery, conjugate point correspondence is not required. Furthermore, without necessarily knowing their absolute location on the ground, linear

features and their inherent constraints could contribute significantly to a solution by reducing the ground control requirements (Weerawong, 1995).

Similarly, linear features can be used as control data for linear scanner imaging systems. Straight lines in object space may appear wavy in airborne linear scanner imagery due to changes in the system trajectory. This deformation of the linear features provides detailed information about the platform trajectory so that changes in the sensor orientation could be detected and estimated.

The Hyperspectral Digital Imagery Collection Experiment (HYDICE) sensor is an airborne pushbroom imaging spectrometer with 210 spectral channels ranging from 0.4 to 2.5 μm (Table 1). With 210 spectral bands for each pixel location, HYDICE provides very accurate land cover classifications.

* Corresponding author.

E-mail address: changno@etri.re.kr (C. Lee).

Table 1
HYDICE sensor characteristics

System attribute	Specification
Platform	ERIM CV-580
Sensor system	2000–7500 m;
operating altitude	6000 m (design point)
Aircraft operating altitude	Sea level–7500 m
V/H (aircraft limits)	0.0127–0.059 rads/s
Optics	Paul Baker foreoptics Schmidt prism spectrometer
Aperture diameter	27 mm
System f/number	3.0
Swath width	308 pixels
Swath FOV	8.94°
IFOV	0.507 mrad (average)
Array size	320 × 210 pixels
Pixel size	40 × 40 μm

However, this data could only be made useful if the geometric relationship between pixels in the image and their corresponding locations on the ground were known.

This paper focuses on the use of straight linear feature for the geometric corrections of the airborne pushbroom imagery. Linear features could be extracted using automated tools in image space and could provide the detailed information to correct the distortions in the raw imagery (Bethel et al., 2000).

2. Sensor and platform model

2.1. Sensor model

Fig. 1 shows the geometric relationship between the ground point and image point of HYDICE imagery for a given scan line. From Fig. 1, the collinearity equation could be derived easily as in frame photography (Mikhail et al., 2001).

$$F_x = 0 + fl \frac{U}{W} = 0 \quad (1)$$

$$F_y = y + fl \frac{V}{W} = 0 \quad (2)$$

where

$$\begin{bmatrix} U \\ V \\ W \end{bmatrix} = \mathbf{M} \begin{bmatrix} X - X_L \\ Y - Y_L \\ Z - Z_L \end{bmatrix} \quad (3)$$

$$\mathbf{M} = \begin{bmatrix} m_{11} & m_{12} & m_{13} \\ m_{21} & m_{22} & m_{23} \\ m_{31} & m_{32} & m_{33} \end{bmatrix}$$

y : coordinate of image point in image coordinate system; X, Y, Z : coordinates of object point in ground coordinate system; X_L, Y_L, Z_L : coordinates of instantaneous perspective center in ground coordinate system; \mathbf{M} : 3×3 orthogonal rotation matrix from ground coordinate system to image coordinate system; fl : calibrated focal length of the sensor.

Note that the six Exterior Orientation (EO) parameters in Eqs. (1) and (2), consisting of three coordinates (X_L, Y_L, Z_L) of the instantaneous perspective center position and three independent rotational angles (ω, φ, κ) implicit in \mathbf{M} , have different values for each scan line. A tremendous amount of control data would be required in order to recover their values.

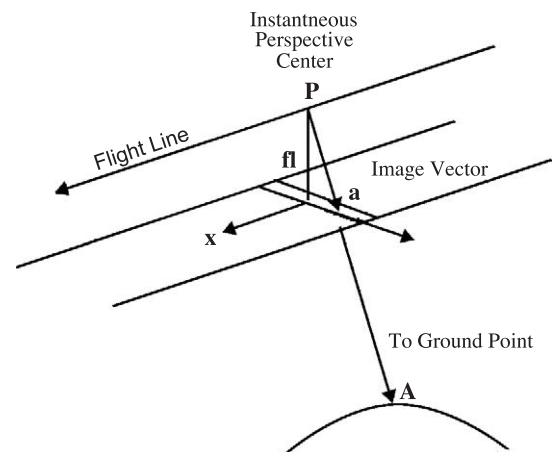


Fig. 1. Collinearity condition.

This problem could be addressed by using a priori information describing the platform trajectory behavior.

2.2. Platform model

The estimation of sensor position and attitude parameters in cases of linear scanner imagery is very closely related to the problem of platform trajectory estimation.

Even though the HYDICE sensor may encounter severe air stream turbulence during its flight, the Flight Stabilization Subsystem (FSS) preserves the sensor optical axis within 1° of nadir when the aircraft pitch and roll angles are within 5° of level flight. The time interval between two adjacent scan lines is very short (8.3–50 ms) (Mitchell, 1995). Therefore, each of the six exterior parameters may change slowly as the line number increases. In addition, each EO parameter in a given scan line should be highly correlated to that in a neighboring scan line.

The Gauss–Markov (GM) process describes these properties well. In this approach, each EO parameter is regarded as a Gauss–Markov process. The parameter for each image scan line is tied or constrained stochastically to other image lines in close proximity. Ethridge (1977) and McGlone et al. (1979) investigated the Gauss–Markov model with airborne MSS data.

Based on the GM process, “pseudo observation equations” could be written for each EO parameter set starting with the second line (Lee et al., 2000; McGlone and Mikhail, 1981), as shown in:

$$F_G = e^{-s_p} \cdot \Delta P_{i-1} - \Delta P_i = 0, \quad (4)$$

where i = line number in the image ($i=2, 3, \dots, n$); s_p = coefficient for each EO element; ΔP is the correction of any EO parameter ($X_L, Y_L, Z_L, \omega, \phi, \kappa$).

Eq. (4) could be considered as fictitious observations with zero values and could be added to the conventional observations. In this equation, the correlation of EO parameters in two adjacent lines is determined by the value of s . If s is close to 0, EO parameters in the adjacent lines are highly correlated. Since the time interval between two adjacent scan lines is very short, s should be close to 0. Various

values were tested to select an optimal value for s . $1e-5$ was chosen and applied to all the EO parameters in the experiments.

Note that the GM process was applied to the corrections of the six EO elements instead of the six elements themselves.

As the number of observed points corresponding to control points or linear features increases, the redundant measurements could contribute significantly to the recovery of EO elements in the vicinity of the observation. This effect could occur if the weights assigned to the constraint equations of GM process were low enough to allow the parameters to vary significantly from one line to the next.

3. Exploitation of linear features

A lot of work is involved in linear feature extraction from digital imagery. Although the term ‘linear feature’ encompasses any continuous feature with a negligible width and includes such parameterizations as splines, this experiment is concerned with the special straight-line case in the object space. The straight lines suffer worst from roll-induced displacements. They occur mainly in the direction of the flight line for the airborne linear scanner imaging system. The lines in the image space can be easily extracted by a semi-automatic approach and used for sensor modelling with appropriate line models.

3.1. Semi-automated line extraction

Manually digitizing points on the line is a time-consuming and error-prone work. Fortunately, this time-consuming work can be replaced by a semi-automatic method, which extracts lines automatically that are given an initial approximate delineation (Gruen and Li, 1995).

The method used in this paper was based on time-delayed, discrete dynamic programming for energy minimization of an active contour (Amini et al., 1990). To start, an initial line was determined approximately. The position of the line was updated by the influence of image gradients near the edge and by the internal smoothness of the line. The update continued until the change in the estimated line position was insignificant.

An energy minimization model has often been used to extract linear features (Kass et al., 1988; Mayer et al., 1997; Klang, 1998). The typical objective function of such an energy-minimizing model can be expressed by the equation:

$$\text{Min. } E = \sum_{i=1}^n [E_{\text{int}}(P_i) + E_{\text{edge}}(P_i)] \quad (5)$$

where

$$E_{\text{int}}(P_i) = (\alpha |P_i - P_{i-1}|^2 + \beta |P_{i+1} - 2P_i + P_{i-1}|^2), \quad (6)$$

$E_{\text{int}}(p_i)$ = internal energy; $E_{\text{edge}}(p_i)$ = energy function related to image gradient; p_i = position (x,y) of i th point on the line; α , β = relative positive weights of each energy term.

This function consists of two energy functions—internal energy and edge energy. Internal energy serves as the force that makes the line smooth. The first term of internal energy is used to make the consecutive points evenly spaced and to keep them from grouping on some areas. The second term makes the shape of the line smooth. Edge energy represents

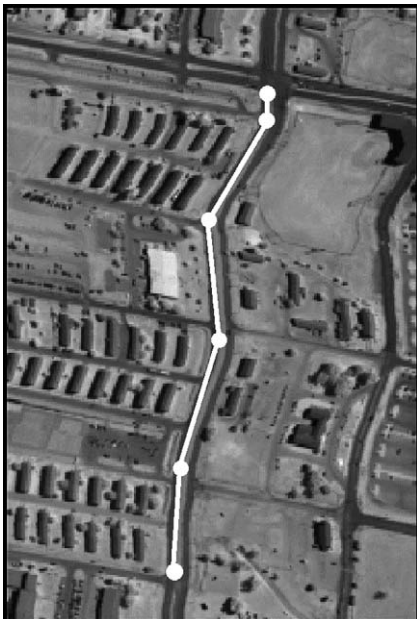


Fig. 2. Initial points on a line.



Fig. 3. Extracted line.

the force that makes the line take the shape of the salient edge features present in the image. Thus, the line is attracted to image points with high gradient values. First, one image band was selected by visual inspection. Then, image gradients were computed using Roberts operator and linearly stretched ranging from 0 to 1000 for normalization. The edge energy for a given line is the sum of gradients of the points on the line.

Dynamic programming was used to update the position of the line. In this method, the problem was divided into a sequence of smaller sub-problems. These problems could then be solved recursively one at a time. Therefore, the computational effort could be reduced significantly.

First, initial points on a line were determined manually (Fig. 2). For each point, the “line” coordinate was fixed and only the “column” value was updated. This was because every scan line, through which a given linear feature passed, had one point of a linear feature. This was a consequence of unique circumstances where the linear features were approximately parallel to the column direction. Next, the initial line was updated within a certain range using dynamic programming. Fig. 3 shows the resulting extracted line using this method.

3.2. Linear feature modelling

Linear features can be used either as control data or as constraint. For the control linear features, ground information of the linear features is needed. On the other hand, for constraints, ground information is not required theoretically.

For the control linear features, two models—the parametric model and the coplanarity model—were investigated. Linear features in the object space could be represented by two end points when they were used for control data. This representation was useful because 3D coordinates of two end points could be easily obtained from surveying data and the consequent observation equations are simple. For the constraint lines, only four out of six parameters were estimated for single image coverage.

3.2.1. Parametric line model

In the parametric form, each coordinate (X,Y,Z) of a point along a line is expressed in terms of an independent parameter, u , associated with the accumulated length along the line between two end points, corresponding to u being equal to 0 and 1 for initial approximations, respectively. Then, Eq. (7) could be used in the collinearity equations (Eqs. (1) and (2)) for each point on the line.

$$\left. \begin{aligned} X &= a_0 + a_1u \\ Y &= b_0 + b_1u \\ Z &= c_0 + c_1u \end{aligned} \right\} \quad (7)$$

where $0 \leq u \leq 1$, $a_0, a_1, b_0, b_1, c_0,$ and c_1 are line descriptors.

Line descriptor parameters $(a_0, a_1, b_0, b_1, c_0, c_1)$ can be computed from the two end points of the line using:

$$[a_0 \ b_0 \ c_0] = [X_1 \ Y_1 \ Z_1], \quad (8)$$

$$[a_1 \ b_1 \ c_1] = [X_2 - X_1 \ Y_2 - Y_1 \ Z_2 - Z_1], \quad (9)$$

where (X_1, Y_1, Z_1) =ground coordinates of an end point on a line; (X_2, Y_2, Z_2) =ground coordinates of the other end point on a line.

The resulting observation equations were nonlinear, as are most estimation problems in practice. These nonlinear equations were linearized and solved using Newton’s root solving method. Linearization of parametric line model can be performed as in conventional frame applications (Mikhail et al., 2001). For line parameter u , the partial derivative can be computed as follows:

$$\frac{\partial}{\partial u} [U \ V \ W]^T = M[a_1 \ b_1 \ c_1]^T \quad (10)$$

$$\partial F_{xi} / \partial u = \frac{fl}{W} \left(\frac{\partial U}{\partial p} - \frac{U}{W} \frac{\partial W}{\partial p} \right) \quad (11)$$

$$\partial F_{yi} / \partial u = \frac{fl}{W} \left(\frac{\partial V}{\partial p} - \frac{V}{W} \frac{\partial W}{\partial p} \right) \quad (12)$$

Similarly, other partial derivatives can be derived for the six EOs and the focal length.

3.2.2. Coplanarity line model

In this model, the coplanarity condition (Fig. 4) is used for the mathematical model of linear features instead of the collinearity condition in the parametric

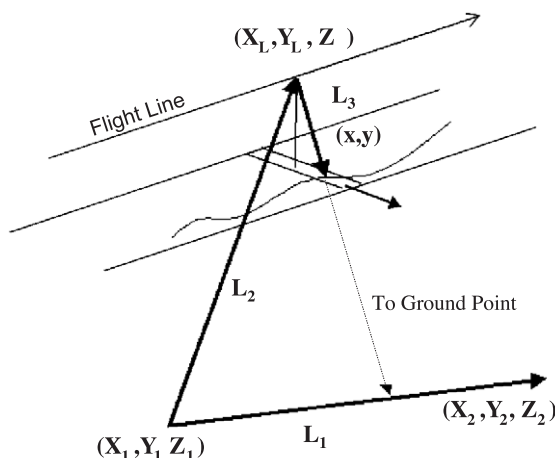


Fig. 4. Coplanarity condition.

model. In Fig. 4, three vectors—a vector ($L1$) along the line, a vector ($L2$) connecting one end point of the line and perspective center, and image vector ($L3$)—should be on the same plane. The coplanarity equation for control lines can be expressed in the form of a determinant as follows:

$$F_L = |L1 \ L2 \ L3| = 0, \tag{13}$$

where: $L1=[X_2-X_1 \ Y_2-Y_1 \ Z_2-Z_1]^T$, $L2=[X_L-X_1 \ Y_L-Y_1 \ Z_L-Z_1]^T$, $L3=M^T[x \ y/f]^T=[u \ v \ w]^T$.

In the coplanarity approach, each point on a control line contributes a single observation equation without the additional line parameter u . Partial derivative for X_L can be computed as follows:

$$\frac{\partial}{\partial X_L}(L_1) = [0 \ 0 \ 0]^T \tag{14}$$

$$\frac{\partial}{\partial X_L}(L_2) = [1 \ 0 \ 0]^T \tag{15}$$

$$\frac{\partial}{\partial X_L}(L_3) = [0 \ 0 \ 0]^T \tag{16}$$

$$\frac{\partial}{\partial X_L}(|L1 \ L2 \ L3|) = \left| \frac{\partial L1}{\partial X_L} \ L2 \ L3 \right| + \left| L1 \ \frac{\partial L2}{\partial X_L} \ L3 \right| + \left| L1 \ L2 \ \frac{\partial L3}{\partial X_L} \right| \tag{17}$$

Similarly, other partial derivatives can be derived for six EOs and the focal length.

3.2.3. Constraint line model

When linear features are used as control data, a line in the object space can be represented by six parameters from 3D coordinates of two end points. However, it is infeasible to estimate the six parameters of the line in the object space from image points of the line for single coverage of pushbroom imagery even though each scan line is considered as single frame geometry. Only four out of six variables can be estimated. Therefore, one coordinate (X or Y) was

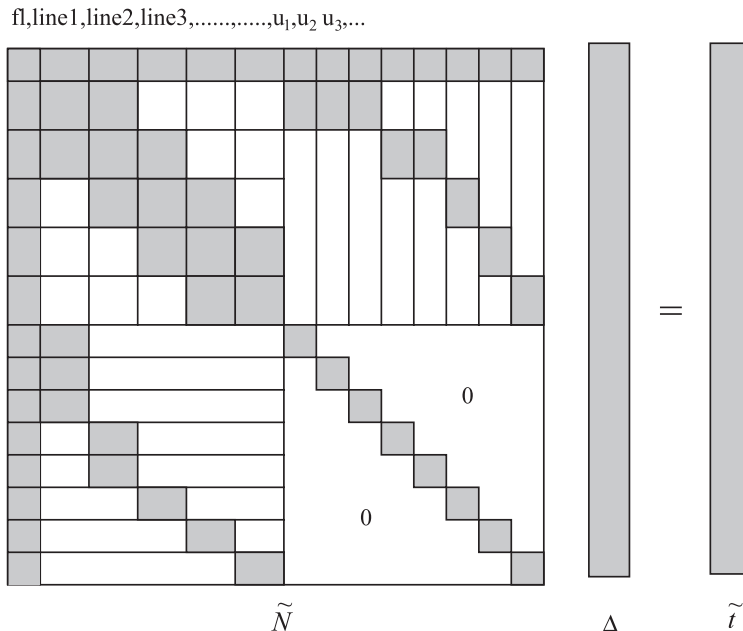


Fig. 5. Pattern of nonzero elements for the normal matrix equation related to the parametric line model.



Fig. 6. HYDICE imagery data set I (Washington, DC).

fixed from two 3D coordinates (X , Y , Z) of end points depending on the flight directions of the data sets. If the flight direction was east–west (X), then Y (south–north) was fixed to initial value, which is computed from initial values of parameters. This representation is simple and similar to the parametric line model. Even though one of the plane coordinates was fixed, the Z values for two end points were difficult to estimate from a single coverage of pushbroom imagery. Consequently, only one coordinate (X or Y) for each end point of a line in the object space was carried and free to adjust as unknown parameter. In the meantime, Z values were carried as unknown parameters but constrained to be close to initial values. The constraint line model can be used as in the parametric line model.

In addition to six EOs, a focal length, and line parameter (u), partial derivatives were needed for coordinates of two end points of lines in object space. For example, the partial derivative for Y_1 (Y coordi-

nate of one end point of a constraint line) can be computed as Eq. (18). Then, the partial derivative for the observation equation can be obtained from Eqs. (10) and (11).

$$\frac{\partial}{\partial Y_1} [U \ V \ W]^T = (1 - u)[m_{12} \ m_{22} \ m_{32}]^T \quad (18)$$

3.3. Implementation

In the proposed models, all the six EO parameters were carried for each scan line and one focal length for the whole image lines. The whole equations could be divided into two groups, namely, observation equations from point and line features, and fictitious observation equations from the Gauss–Markov process.

For the adjustment, the unified approach was used for all the models. In this approach, all the parameters



Fig. 7. HYDICE imagery data set II (Fort Hood).

were assumed as observations. For unknown parameters, each parameter was considered as an observation with infinitely large variance or equivalently zero weight. Then it was allowed to change freely in the adjustment. For the constraint, an observation was introduced with a very large weight so that it was unlikely to be changed in the adjustment (Mikhail et al., 2001).

Unknown parameters could be solved iteratively with initial approximations. Only one value for each angle was used for the entire scan lines as initial approximations, while each scan line had different values for position parameters. Initial values for the ω and φ angles were set to 0. The initial value for κ angle was estimated from the control points. For position parameters, the initial values were obtained by linear interpolation from GPS data because GPS data were not available for each scan line. The position parameters were introduced with relatively high weights so that final results were close to the initial approximations computed from GPS data in the adjustment.

In this research, all the six EO parameters for entire scan lines were carried as unknown parameters. Consequently, inversion of a huge matrix was needed. However, the matrix had a well-defined structure. Furthermore, by eliminating one set of variables, the size of the matrix could be reduced. After solving for remaining parameters, the other parameters could be solved by back-substitution (Mikhail et al., 2001).

Table 2
Contribution of control lines

Case no.	Point density	Check point RMS (m)			
		Washington, DC		Fort Hood	
		ΔX	ΔY	ΔX	ΔY
1	Points only	1.95	1.99	1.61	2.30
2	Every 16th point on lines	1.98	1.66	1.48	1.41
3	Every 8th point on lines	1.98	1.61	1.48	1.36
4	Every 4th point on lines	1.98	1.59	1.49	1.32
5	Every 2nd point on lines	1.98	1.60	1.49	1.31
6	Every point on lines	1.98	1.61	1.49	1.32

Table 3
Comparison between different line models

Line model	Check point RMS (m); Washington, DC		Check point RMS (m); Fort Hood	
	ΔX	ΔY	ΔX	ΔY
Point only	1.95	1.99	1.61	2.30
Parametric	1.98	1.61	1.49	1.32
Coplanarity	1.98	1.61	1.50	1.32
Constraint	1.93	1.92	1.65	1.26

For the parametric line model, the related equations can be expressed as:

$$\begin{bmatrix} v \\ v_G \\ v_x \end{bmatrix} + \begin{bmatrix} B \\ G \\ -I \end{bmatrix} \Delta = \begin{bmatrix} f \\ 0 \\ f_x \end{bmatrix}, \quad (19)$$

where v, v_G, v_x =residual vectors for observation (control points and lines), Gauss–Markov process, parameter equations in unified approach; B =matrix of partial derivatives for unknown parameters; G =matrix of coefficients for parameter corrections in Gauss–Markov process; Δ =a vector for the corrections of unknown parameters; f =a vector

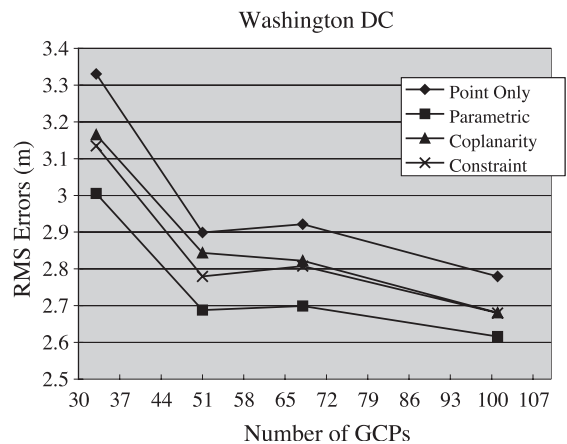


Fig. 8. Planimetric RMS errors of check points with various control point configurations (Washington, DC).

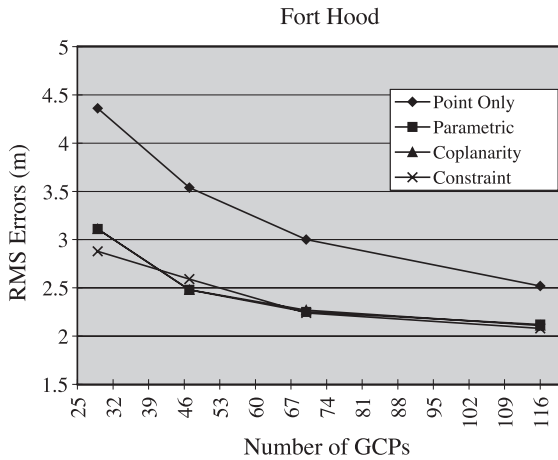


Fig. 9. Planimetric RMS errors of check points with various control point configurations (Fort Hood).

for computed image coordinates—observed image coordinates

$$\left(-f_l \frac{U}{W} - x \text{ or } -f_l \frac{V}{W} - y \right)$$

f_x = a vector for updated parameters—initial approximations of parameters. Then, the corresponding normal equations are

$$[N + N_G + W_{xx}] \Delta = [t - W_{xx} f_x], \tag{20}$$

where $N = B^T W B$, $N_G = G^T W_G G$ and $t = B^T W f$.

W, W_G, W_{xx} = weight matrices for observations, fictitious observations from Gauss–Markov process, and parameters in unified approach.

The pattern of nonzero elements for the normal matrix equation with the parametric line model is shown in Fig. 5. First, eliminating the line parameters (u) reduced the normal equations. Then, the reduced

normal equations had the same pattern of upper-left part of original normal equations (Fig. 5). In succession, the six EO parameters were eliminated line by line until the number of the remaining parameters was small enough for matrix inversion. Once the remaining parameters were computed with the reduced normal equations, other parameters could be solved by back-substitution.

4. Experiments

4.1. HYDICE images

Two HYDICE images were used in this research. Both images had 320 samples \times 1280 lines. The first data set was collected over the Washington, DC mall in August 1995. Its ground sample distance was about 3.2 m and the scale was approximately 1:80,000. Its flight height was about 6320 m. From Fig. 6, the straight line features, such as roads and building edges, along the flight direction display a modest degree of roll-induced “waviness”.

The second data set was flown over the urban area of Fort Hood, TX, in October 1995. Its nominal scale and ground sample distance were 1:56,000 and 2.2 m, respectively. Its flight height was about 4430 m. As can be seen from Fig. 7, straight roads along the in-track direction were severely “wavy”.

In addition to image data, support information was available for each scan line of HYDICE image. These support data consist of inertial navigation system (INS) data, Global Positioning System (GPS) data, Flight Stabilization Subsystem (FSS) pointing knowledge, and engineering data. Unfortunately, the use of INS/FSP angular data did not prove helpful when used as a priori information. Perhaps this was due to



Fig. 10. Ortho-rectified image (points only, Washington, DC).



Fig. 11. Ortho-rectified image (points and lines, Washington, DC).

excessive dynamic effects, timing offsets, or coordinate system inconsistencies, to name a few possibilities. Other airborne pushbroom systems have apparently been able to profitably exploit such INS data to reduce control requirements on the ground (Bruton et al., 2001).

4.2. Control and check data

To determine the parameters of the sensor model, both image coordinates and ground coordinates were needed for control data. The performance was evaluated using separate check data. The ground coordinates were commonly obtained from a conventional field survey or a GPS survey. In the data sets, however, the ground coordinates of point data and the end points of the lines were obtained from triangulated aerial frame photography.

For the Washington, DC area, a total of 202 points were extracted from the frame photography on the digital photogrammetric workstation. The same 101 check points were used in all of the experiments, with the other 101 control points available for the HYDICE restitution. Similarly, a total of 232 points were

extracted for Fort Hood area. The same 116 check points were used in all of the experiments, leaving up to 116 control points available for the HYDICE restitution.

The extracted straight lines generally fell into two categories, namely, road boundaries and building sides. Band 80 was chosen for both data sets because the linear features of interest had visually the best contrast in this band. Image gradients were computed and linearly stretched ranging from 0 to 1000. For the values of α and β , various values were tested and $\alpha = \beta = 100$ was the most suitable in the test. However, the results of different sets were similar. For the Washington, DC area, 50 straight linear features were extracted from the HYDICE imagery. Similarly, 73 lines were extracted for the Fort Hood area.

4.3. Adjustment results

In order to quantify the performance of each model, the root mean square (RMS) residuals of check points were examined. Since only single image coverage was available, the Z coordinate had to be fixed to its known value.

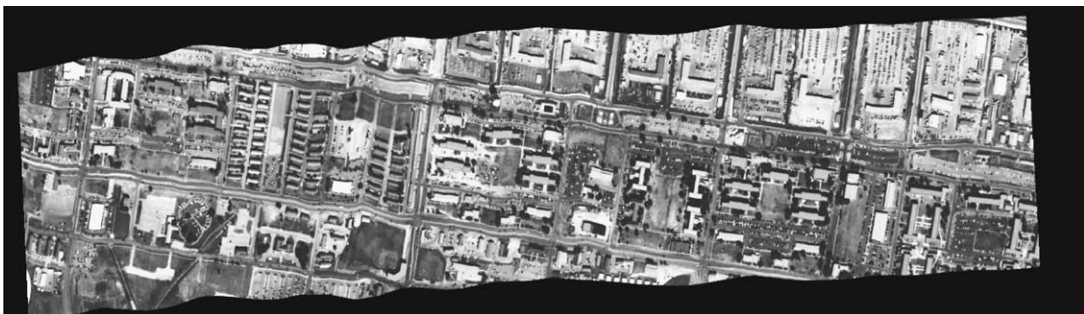


Fig. 12. Ortho-rectified image (points only, Fort Hood).

Experiments were run to compare the accuracy obtained from the restitution of HYDICE imagery using different control features. First, only control points were used to determine the unknown parameters. Next, the experiments were repeated with lines in addition to control points. Two data sets showed similar results. Adding control line features to the solution improved ΔY (cross track) of check points significantly, while ΔX (along track) of check points were essentially the same (Table 2).

The contribution of linear features was examined with a varying density of points on the control linear features. First, only control points were used to determine the unknown parameters. Next, the experiments were repeated as the density of the points on the control lines was increased and the coplanarity line model was used for the linear features. Two data sets showed similar results. Adding straight line features to the solution improved ΔY of check points and check lines significantly, while ΔX of check points were essentially the same. In particular, when the image had severe distortions, the benefit of linear feature was more significant (Table 2). However, the benefit of adding additional linear feature points was reduced as the density of points on the lines increased.

Another experiment was performed to compare the performance of the three line models. In addition to control points, linear features with different models used as control data and the RMS residuals of check points were computed. The difference between the parametric model and the coplanarity model was insignificant for both data sets (Table 3). However, RMS residuals showed different results for the constraint line model. The contribution of the constraint linear features was insignificant for the Washington,

DC data set. On the other hand, restitution accuracy was significantly improved for the Fort Hood data set.

Because the number of control points and control/constraint linear features was high in the above experiments, experiments were performed to investigate the relationship between the restitution accuracy and the number of control points. This was done by changing the number of control points with a fixed number of linear features. For both data sets, the same 24 lines were used for different line models, while the number of control points was changed. Figs. 8 and 9 show the planimetric errors with different control point configurations and different line models using the same check points in the previous experiments. When the number of control points was low, the RMS residuals were rapidly improved for all four different cases (control points only and three line models) as the number of control points was increased. The contribution of the linear features was more significant for the Fort Hood data set as in the previous experiments.

4.4. Ortho-rectified images

In addition to supporting the effectiveness of the linear features with tables of numerical results, ortho-rectified images could also be used to visually compare the results of different control features. First, ortho-rectification was performed with control points only. Next, both control points and lines were used to create ortho-rectified images. Figs. 10 and 11 show the ortho-rectified images of the Washington, DC area with different control features. The straightness of the roads in the ortho-rectified image with linear features could be noted and compared to the visible wiggles in



Fig. 13. Ortho-rectified image (points and lines, Fort Hood).

the others. For the Fort Hood area, the difference between the two images could be distinguished more. The severe wiggles along the flight line still remained in the ortho-rectified image with control points only (Fig. 12), while they were almost eliminated in the ortho-rectified image with linear features (Fig. 13).

5. Conclusions

The ability to accurately recover values for the time-dependent EO parameters of the sensor was enhanced by the contribution of linear features. Because of the flexibility of the Gauss–Markov process as the platform model, the number of observations or the density of observations with respect to the scan lines contributed to the performance of the model. The severe distortions along the flight line were almost eliminated in the ortho-rectified image with linear features.

The difference between the parametric and coplanarity line models was insignificant. The basic theories of these models were essentially the same. Therefore the corresponding results were similar. However, the coplanarity model required a smaller number of parameters. Consequently, its implementation was simpler than that of the parametric model. The constraint line model also showed good performance when the image had severe distortions.

Because of the lack of information about the INS angular data, further investigation was not performed for the use of GPS/INS data in this research. The integration of INS/GPS data and image measurements may simplify the sensor and platform modelling and reduce the control data requirements significantly. Therefore, it is recommended to investigate INS/GPS data integrated with image measurements.

Acknowledgements

This research was supported by the U.S. Army Research Office (ARO) through a Multidisciplinary University Research Initiative (MURI) project titled “Rapid and Affordable Generation of Terrain and Detailed Urban Feature Data” under Grant No. DAAH04-96-1-0444. The authors acknowledge the director of the project, Professor Edward M. Mikhail, who also reviewed this paper.

References

- Amini, A., Weymouth, T., Jain, R., 1990. Using dynamic programming for solving variational problems in vision. *IEEE Transactions on Pattern Analysis and Machine Intelligence* 12 (9), 855–867.
- Bethel, J., Lee, C., Landgrebe, D., 2000. Geometric registration and classification of hyperspectral airborne pushbroom data. *International Archives of Photogrammetry and Remote Sensing* 33 (Part B7), 183–188.
- Bruton, A.M., Mostafa, M.M.R., Scherzinger, B., 2001. Airborne DGPS without dedicated base stations for mapping applications. *Proceedings of ION-GPS 2001*, 1584–1591.
- Ethridge, M.M., 1977. Geometric Analysis of Singly and Multiply Scanned Aircraft Digital Data Arrays. PhD Thesis, School of Civil Engineering, Purdue University, West Lafayette, IN.
- Gruen, A., Li, H., 1995. Road extraction from aerial and satellite images by dynamic programming. *ISPRS Journal of Photogrammetry and Remote Sensing* 50 (4), 11–20.
- Habib, A., Asmamaw, A., Kelley, D., May, M., 2000. Linear features in photogrammetry. Report, vol. 450. Department of Civil and Environmental Engineering and Geodetic Science, The Ohio State University, Columbus, OH.
- Kass, M., Witkin, A., Terzopoulos, D., 1988. Snakes: active contour models. *International Journal of Computer Vision* 1 (4), 321–331.
- Klang, D., 1998. Automatic detection of changes in road databases using satellite imagery. *International Archives of Photogrammetry and Remote Sensing* 32 (Part 4), 293–298.
- Lee, C., Theiss, H., Bethel, J., Mikhail, E., 2000. Rigorous mathematical modelling of airborne pushbroom imaging systems. *Photogrammetric Engineering and Remote Sensing* 66 (4), 385–392.
- Mayer, H., Laptev, I., Baumgartner, A., Steger, C., 1997. Automatic road extraction based on multi-scale modeling, context, and snakes. *International Archives of Photogrammetry and Remote Sensing* 32 (Part 3), 106–113.
- McGlone, J.C., Mikhail, E., 1981. Photogrammetric analysis of aircraft multispectral scanner data. Technical Report. School of Civil Engineering, Purdue University, West Lafayette, IN.
- McGlone, J.C., Baker, J.R., Mikhail, E.M., 1979. Metric information from aircraft multispectral scanner (MSS) data. *Proceedings of the 45th Annual Meeting, American Society of Photogrammetry*, Washington, DC, pp. 274–289.
- Mikhail, E.M., Bethel, J.S., McGlone, J.D., 2001. *Introduction to Modern Photogrammetry* Wiley, New York, NY.
- Mitchell, P.A., 1995. Hyperspectral digital imagery collection experiment HYDICE. *Proceedings of SPIE* 2587, 70–95.
- Mulawa, D., 1989. Estimation and photogrammetric treatment of linear features. PhD Thesis, School of Civil Engineering, Purdue University, West Lafayette, IN.
- Sayed, A.N., 1990. Extraction and Photogrammetric Exploitation of Features in Digital Images. PhD Thesis, School of Civil Engineering, Purdue University, West Lafayette, IN.
- Weerawong, K., 1995. Exploitation of Linear Features for Object Reconstruction in Digital Photogrammetric Systems. PhD Thesis, School of Civil Engineering, Purdue University, West Lafayette, IN.